REPORT DOCUMENTATION PAGE

AFRL-SR-BL-TR-99-

0137

1. AGENCY USE ONLY *(Leave blank)*	2. REPORT DATE	3. REPORT TYPE AND DATES COVERED
	May 1999	FINAL REPORT 1 Feb 97 - 30 Apr 99

4. TITLE AND SUBTITLE
AN EXPERIMENTAL STUDY OF SUPERSONIC FLOWS OVER AN ELLIPTIC CONE

5. FUNDING NUMBERS
F49620-97-1-0088

61102F
2307/AS

6. AUTHOR(S)
M. SAMIMY, J. I. HILEMAN, AND J.-H. KIM

7. PERFORMING ORGANIZATION NAME(S) AND ADDRESS(ES)
OHIO STATE UNIVERSITY
MECHANICAL ENGINEERING
COLUMBUS, OH 43210

8. PERFORMING ORGANIZATION REPORT NUMBER

9. SPONSORING/MONITORING AGENCY NAME(S) AND ADDRESS(ES)
AIR FORCE OFFICE OF SCIENTIFIC RESEARCH (AFOSR)
801 N. RANDOLPH STREET, ROOM 732
ARLINGTON, VA 22203-1977

10. SPONSORING/MONITORING AGENCY REPORT NUMBER

11. SUPPLEMENTARY NOTES

12a. DISTRIBUTION AVAILABILITY STATEMENT
APPROVED FOR PUBLIC RELEASE, DISTRIBUTION IS UNLIMITED

12b. DISTRIBUTION CODE

13. ABSTRACT *(Maximum 200 words)*

An elliptic cone similar to the one used by other investigators, a 4:1 aspect ratio elliptic cone with the cone angle on the major axis of 17.5o and 4.5o along the minor axis, in a Mach 2.8 tunnel was used in the present work. The Reynolds number used in this work was much higher than that used in other experimental work. The purpose is to examine the transition proces as well as the turbulent structure of a three-dimensional boundary layer after transition. The primary focus of this study is on the structure of the turbulence, which was explored using advanced optical diagnostics. Both surface flow visualizations and Filtered Rayleigh Scattering (FRS_) based flow visualizations were used in this study. The rsults showed that the boundary layer developing along the major centerline, the flattest region on the cone surface, underwent transition to turbulence approximately 35 mm downstream of the cone tip. Surface cross flow was observed primarily near the minor centerline of the cone, the area with the largest curvature. No cross flow was observed around the major centerline after 10 mm downstream of the cone tip.

14. SUBJECT TERMS	15. NUMBER OF PAGES
	31
	16. PRICE CODE

17. SECURITY CLASSIFICATION OF REPORT	18. SECURITY CLASSIFICATION OF THIS PAGE	19. SECURITY CLASSIFICATION OF ABSTRACT	20. LIMITATION OF ABSTRACT
UNCLASSIFIED	UNCLASSIFIED	UNCLASSIFIED	

An Experimental Study of Supersonic Flows Over an Elliptic Cone

M. Samimy*, J. I. Hileman**, and Jin-Hwa Kim***
Department of Mechanical Engineering
The Ohio State University
Columbus, Ohio 43210

Final Technical Report
(MEMS-99-101)

For

AFOSR Grant F49620-97-1-0088

For the Period of

February 1, 1997 to April 30, 1999

May 1999

---

* Principal Investigator, Professor and Associate Chairman
** Graduate Student
*** Postdoctoral Researcher

ABSTRACT

Over the past several years, there have been a limited number of experimental, computational, and theoretical activities on transitional three-dimensional boundary layers formed over a cone with an elliptic cross section. An elliptic cone similar to the one used by other investigators, a 4:1 aspect ratio elliptic cone with the cone angle on the major axis of 17.5° and 4.5° along the minor axis, in a Mach 2.8 tunnel was used in the present work. The Reynolds number used in this work was much higher than that used in other experimental work. The purpose is to examine the transition process as well as the turbulent structure of a three-dimensional boundary layer after transition. The primary focus of this study is on the structure of the turbulence, which was explored using advanced optical diagnostics. With mutual agreement of the AFOSR and the Principal Investigator, the research direction was changed midway through the research. Therefore, this final report only presents some of the preliminary findings of the research program.

Both surface flow visualizations and Filtered Rayleigh Scattering (FRS) based flow visualizations were used in this study. The results showed that the boundary layer developing along the major centerline, the flattest region on the cone surface, underwent transition to turbulence approximately 35 mm downstream of the cone tip. Surface cross flow was observed primarily near the minor centerline of the cone, the area with the largest curvature. No cross flow was observed around the major centerline after 10 mm downstream of the cone tip. The FRS flow visualizations showed that after transition had occurred the flow was dominated by large structures in the developing region of the turbulent boundary layer. The developing boundary layer was random in nature; meaning that there was not a consistently measurable boundary layer on the surface. Farther downstream, it appeared to be similar to a two-dimensional supersonic boundary layer. The boundary layer was thicker at the centerline; however, a bulging of the boundary layer at the centerline, which had been observed by previous researchers in higher Mach number experiments, was not noticed in the present experiments.

[ ] - abstract.

INTRODUCTION

Over the past three decades, there has been sporadic work in both high supersonic and hypersonic three-dimensional boundary layers. However, the nature of transition and subsequent turbulence structure is not well understood in such flows. Within the past several years, there have been some focused activities on three-dimensional boundary layers in both the theoretical/computational front (Reed and Haynes, 1994, Huang et al., 1995, Lyttle and Reed, 1995, and Kimmel et al. 1997) as well as the experimental front (King et al., 1992, Cattafesta et al., 1995, Schneider et al., 1996, and Smits, 1997). Regarding the experimental high supersonic three-dimensional boundary layer work, which is also the subject of the present research, quiet-flow tunnels have been used to study transition in a Mach 3.5 flow over a cone with an angle of attack (King, 1992), a Mach 3.5 flow over a swept wing (Cattafesta et al., 1995), and a Mach 4 flow over an elliptic cone (Schneider et al., 1996).

There are two main findings in these cited references. First, the cross flow instability seems to be the dominant stability mode in the three-dimensional boundary layer whether the flow is over a swept wing or an elliptic cone. Second, there seems to be a major difference regarding the Reynolds number at which turbulent transition takes place over an elliptic cone between the computational/theoretical models and experimental work. The predicted transitional Reynolds number from computational/theoretical models seems to be much smaller than that from experimental work.

The objective of the present work is to use the same elliptic cone geometry that was used by Schneider et al., but in a conventional Mach 2.8 tunnel with a larger Reynolds number. The Reynolds number is over an order of magnitude higher than that used by Schneider et al. Both the transition process and the turbulent structure of the three-dimensional supersonic boundary layer will be examined. The focus of the research will be to explore the turbulent structures using advanced optical diagnostics.

EXPERIMENTAL FACILITY AND TECHNIQUES

Wind Tunnel Facility

The wind tunnel facility is located at the Aeronautical and Astronautical Research Laboratory of The Ohio State University. The wind tunnel is a blow-down facility with air supplied by two four-stage compressors that feed a storage tank with a volume of 1500 ft^3 (42.5 m^3) at a pressure of up to 2380 psi (16.4 MPa). Twin desiccant dryers remove moisture from the air before compression. The tunnel dimensions are six by six inches (152.4 mm x 152.4 mm) at the test section with a flow velocity of about 600 m/s (Mach 2.8) as determined by pressure measurements from a pitot-static probe. Two removable windows are located on each side of the tunnel and measure 17.7 inches (450 mm) in length and 3.15 inches (80 mm) in height. These windows allow viewing of the test section. The top of the tunnel has a window 3 inches (76 mm) wide and 7.5 inches (191 mm) long. It is offset from the tunnel centerline 2.3 inches (58 mm). This window allows the laser sheet to enter the tunnel test section.

Before this research project was started, the tunnel had been used to study the effects of extra rates of strain in a Mach 3 boundary layer (Arnette et al., 1995 & 1998). A splitter plate allowed for a long expansion region, but it also divided the tunnel into half of the possible size. The splitter plate was removed from the tunnel and new floor and ceiling plates were put into place to form the converging-diverging nozzles. These changes brought the tunnel to the dimensions described above.

Elliptical Cone Model

The elliptical cone model has a four-to-one aspect ratio. The cone is 6.3 inches long, 4.0 inches wide and 1.0 inches tall. The angle on the major axis is 17.5°, while it is 4.5° along the minor axis. All components of the cone and its mounting hardware were constructed from aluminum. To reduce light scattering from the model surface, the cone was anodized black. The cone dimensions are shown in Figure 1.

The maximum area that the elliptical cone and supporting hardware could occupy while allowing the tunnel to operate supersonically had to be calculated to come up with the dimensions described above. The tunnel would become choked if the percentage of the wind tunnel cross-sectional area that was blocked by objects were too large, and therefore it would not operate properly. The text by Pope and Goin (1965) contains the empirical relationship $\frac{d_m}{\sqrt{A}} = 0.38$ for a Mach 2.8 flow, where d_m is the equivalent circle diameter for the model, and A is the effective tunnel area. The effective tunnel area is equal to the tunnel cross-sectional area minus the area that is occupied by the boundary layer over the walls of the tunnel. This

relationship was used to calculate the cone dimensions described above, with the length chosen to maintain the major and minor angles used by Schneider et al. (1996).

Initially, the model was supported in the tunnel by a dual-post system as shown in Figure 2. The cone was bolted to an elliptical plate that was attached to a collar that slid over a long, slender support tube, having an inner diameter of 1/2 inch and an outer diameter of 5/8 inch. Post supports measuring 2 inches in length held the tube behind the collar and at its rear. The posts were aerodynamically shaped for minimal drag. They were spaced 13.9 inches apart, had a centerline height of 3.0 inches, and were bolted to plates in the tunnel floor. The tube and collar were bolted together, while the tube was held to the front post by dowel pins.

The cone support structure proved to be insufficient. During tunnel operation, the cone tip vibrated noticeably. The vibrations would interfere with the natural growth and development of the boundary layer. The cone movement was believed to be due to small gaps between the individual components of the support hardware. Creating a new one-piece post mount eliminated this. The new mount design was based upon the front portion of the existing support structure and was machined at the machine shop within the AARL. The updated mount is photographed in Figure 3 with the cone model in the tunnel. No further problems were encountered with cone vibration.

The manufacture of the elliptic cone was performed at the Smith Laboratory machine shop at OSU on a CNC milling machine. Due to limitations inherent with milling operations, the tip of the cone has a diameter of 0.040 inches, which is also the same as that of Schneider et al. (1996). The cone surface was polished after the milling process was completed. To accommodate for pressure taps, the cone had a portion of its inner material removed by another CNC milling operation. The minimum wall thickness of the cone is 0.20 inches.

Surface Flow Visualization Techniques

To investigate the three-dimensional nature of the flow over the cone and to get an approximate location of the transition location, two kinds of surface flow visualization techniques were used. Both techniques are similar in that they use a mixture of very fine powder and a carrier fluid. One technique uses a volatile carrier fluid that evaporates completely during the test, while the other uses a non-volatile carrier fluid as in the conventional oil based technique. The use of a volatile carrier fluid eliminates unfavorable tunnel shut-off effects (Settles and Teng, 1983). The kerosene-lampblack surface streak method, as a volatile fluid based technique, was developed by Settles and Teng (1983). The surface flow on the trailing edge of a rectangular jet was successfully visualized with the use of this technique (Kim, 1998). However, this technique was not successful for the surface flow visualization on the cone. This is probably due to a wide range of shear on the model and the divergence of the surface area in

the main flow direction. With this technique, only the middle region of the top cone surface was visualized.

Thus, as an alternative method, an oil-based surface flow visualization technique was employed. A 1:1:2 mixture, by volume, of Dow Corning 200 Fluid with 500 cS silicone oil, linseed oil, and Windsor & Newton titanium white paint was used to overcome the problem encountered with the kerosene-lampblack technique (Cattafesta et al., 1995). The purpose of using two different viscosity oils is to visualize both high and low shear regions of the side and top surfaces (see Figure 1), respectively, at the same time. The mixture of linseed oil and titanium paint marks the flow pattern in the high shear region of the side surface, while the less viscous mixture of silicone oil and titanium paint leaves flow marks in the low shear region of the top surface. Using either silicone or linseed oil by themselves with the paint resulted in a limited surface flow pattern.

The mixture was uniformly coated on the cone immediately before each test. To minimize start-up and shut-off effects on the flow pattern, the control valve was opened and closed within a second. After running the tunnel 15-20 seconds, the model was taken out of the tunnel and a camera took the image of the flow. The images from the surface flow visualizations were stored to a computer by a scanner with a resolution of 400 pixels per inch.

Filtered Rayleigh Scattering (FRS) Technique

The focus of this research was to investigate the turbulent boundary layer as it forms over the elliptical cone. An optical technique was needed that can take short duration pictures of the flow without visual interference from objects surrounding the flow. A non-intrusive technique was needed to avoid causing disturbances within the layer. High spatial resolution was also desired. With these stipulations, the Filtered Rayleigh Scattering (FRS) technique was chosen for flow visualization.

System Operation

The main components of the experimental arrangement are shown together schematically in Figure 4, and are photographed together in Figures 5. Miles et al. (1990) developed the FRS technique to obtain flow visualizations with suppression of background reflections. The technique utilizes light scattered from small particles to track air movement within the free stream. Either the particles can be seeded into the flow or they could be the molecules that comprise the flow. In this experiment, particles were seeded into the flow.

Light that is scattered from walls, windows, etc. of an experimental system introduces visual noise to any picture taken of the wind tunnel interior. By taking advantage of the Doppler frequency shift that all waves experience when encountering a moving object, one can solve the

problem of having unwanted scattered light. An optical filter is used to discriminate between light that is of a known frequency and light that has been Doppler shifted. With background suppression, visualizations can be made extremely close to the walls surrounding a flow, even in highly reflective backgrounds such as those in wind tunnels.

The filter needs to have notch band absorption of the incident light frequency while transmitting light at the Doppler shifted frequency. The molecular filter profile of the ratio of incident light to transmitted light has a distinct "well" where incident light of a distinct frequency is absorbed, and there are other frequencies where light is transmitted. The incident light is adjusted so its frequency is in the absorption well. Thus, light that has been scattered by moving particles will experience a Doppler frequency shift and will be transmitted through the filter. Light that has been scattered from stationary objects within the wind tunnel will be absorbed because it has a frequency that is in the absorption well.

The Doppler frequency shift is equal to the particle velocity multiplied by a constant that is determined by the orientation of the system, and then divided by the wavelength of the incident light. The Doppler shift is maximized by having the direction of observation be parallel to the motion of the particle, while also being perpendicular to the incident light. Even at this optimum orientation, the shift in wavelength for a 532 nm electromagnetic wave (green visible light as produced by a Nd:YAG laser) for a particle velocity of 600 m/s is only 1.1 GHz. This is very small compared to the frequency of 5.6×10^{14} Hz that accompanies a wavelength of 532 nm. For this reason, a notch-absorption optical filter with a very steep transition from full absorption to transmission is essential for background suppression with the conditions used in this study; a molecular iodine optical filter has such properties.

Optical Filter

The essential feature for the FRS technique is an optical filter that suppresses background light. If the light that is scattered off the metallic parts of the test area is suppressed, then the flow can be resolved to the small spatial dimensions needed for boundary layer visualizations. If the background light were not suppressed, then an observer would only see the very bright reflections off the metallic cone model, wind tunnel walls, and windows; thus, the flow pattern would be lost in the light noise.

As previously stated, the filter is a notch or band-absorption filter to incident light frequency. Iodine vapor inside the cell has distinct absorption bands at wavelengths around 532 nm. This characteristic of iodine makes it appealing for FRS visualizations since Nd:YAG lasers emit light at 532 nm, corresponding to a wave number of 18788.4 cm^{-1}. Theoretical filter profiles for this filter were computed using a computer code written by J. Forkey. An enlarged portion of the theoretical filter profile around the operating range used for this experiment is

shown in Figure 6. The third absorption line, which is at 18788.4 cm^{-1}, was used for background suppression purposes for this experiment.

The filter, shown schematically in Figure 7, is created from blown glass. The glass cylinder is 3.2 inches in diameter and 10 inches long. A small side arm protrudes from the surface of the filter to allow for condensation of the iodine gas if nitrogen pressure broadening were required. An inlet finger with a stopcock allows the addition of iodide to the filter and the evacuation of air from the filter. Another finger on the filter is surrounded by a water jacket. This finger has a stopcock that isolates solid iodine from the main section. The filter has been wrapped with two strands of heater tape, fiberglass insulation, and metallic tape. A K-type thermocouple, placed between the heater tape and glass, measures the filter temperature.

Figure 7 also shows some details of the optical filter preparation. The filter was cleaned internally by blowing nitrogen gas through the stopcock of the inlet finger. This ensured that no water or water vapor was present in the filter to chemically react with the iodine vapor. A small amount of crystallized iodine was inserted into the filter through the inlet finger. A vacuum pump was then attached to the inlet finger. The filter was evacuated and the stopcock was closed, thus sealing the inside of the filter. The relation of iodine pressure, P_{I2}, to the filter temperature, T_{filter}, and the cooling water temperature flowing through the water jacket, T_{I2}, was given (TRC Thermodynamics Tables, 1975) as

$$\log_{10}\left(P_{I_2}\right) = 9.75715 - \frac{2867.028}{\left(254.180 + T_{I_2}\right)}$$

The temperatures were measured in degrees Celsius, while the pressure was in torr. Water at a temperature of 30 ± 0.1°C flowed through the water jacket (T_{filter}), while the filter was heated to 85°C (T_{I2}). The combination of temperatures yielded an iodine vapor pressure (P_{I2}) of 0.47 torr in the main portion of the filter. After the filter had been subjected to a constant T_{filter} and T_{I2} for several hours, the stopcock on the water jacket was closed, and the iodine partial pressure was set.

ICCD Camera

A Princeton Instruments Intensified Charged Couple Device (ICCD) model 576-S camera was used to take all of the FRS images presented in this report. The camera has a resolution of 576 by 384 pixels. The camera was used in bin mode with the individual pixels binned by 2 to form larger super pixels; this yielded an array of 288 by 192. The portion of the CCD array focused on the test section could also be adjusted to include only the portion of the flow that was of interest; the other areas of the array were not active.

The filter could not completely eliminate reflections from the metallic cone surface, so

other measures were also taken to suppress this scattering. The reflections were eliminated in the streamwise visualizations by first mounting the camera on two adjustable stages to allow for precise movement in two directions: vertical and horizontal away from the model. The camera angle was adjusted with respect to the horizontal until it matched the angle of the illuminated cone surface. Thus, the FRS flow visualizations are parallel to the cone surface, not the true horizontal plane. Only the portion of the CCD array that showed flow was used; the portion of the CCD array that showed reflections from the cone surface was not used. This helped to eliminate the surface reflections as well. For the spanwise views, surface reflections were eliminated by carefully placing putty over the portion of the side window of the tunnel that was between the camera and the bright portion of the cone surface.

For optimum spatial resolution without distortion, the camera should be oriented perpendicular to the laser sheet. This yields the most accurate view of the flow features. However, at such an angle the Doppler frequency shift is zero, and background suppression is not possible. As stated earlier, viewing the flow at an angle parallel to the laser sheet yields the maximum Doppler shift. However, this angle will yield no resolution of the flow since the light sheet will appear as a line. To reach a compromise between achieving a large Doppler shift and retaining flow resolution; the camera has been placed at an angle of approximately 45° to the wind tunnel.

Laser

The light source for this experiment is a Continuum 8010 Powerlite pulsed Nd:YAG laser. A high power laser is necessary for FRS experiments due to the low intensity of Rayleigh/Mie scattering. The laser has a repetition rate of 10 Hz. The pulse duration is nine nanoseconds, which is sufficiently short to "freeze" the 600 m/s flow. Any particle within the free-stream moves 0.0054 mm during this time span. An injection-seeded laser is used to reduce the linewidth of the Continuum laser. Without the seeder, the laser has a linewidth on the order of GHz, but with the seeder operating, it is approximately 50 MHz. If the linewidth were not narrow, completely suppressing the background light would not be possible because of the small width of the absorption "well" associated with the iodine filter. The seeder has a finely tunable frequency that is controlled by a voltage input, which allows for exact placement of the laser frequency relative to the optical filter profile.

The laser beam is redirected and formed into a sheet by optics placed on a large lattice structure constructed of tube steel. A series of prisms redirects the beam to the cone model. Once above the cone model, the beam is focused onto the cone surface by a bi-convex lens with a focal length of approximately 40 inches. A cylindrical plano-convex lens stretches the beam into a sheet that can be either parallel or perpendicular to the direction of air movement in the

tunnel. By moving the optics horizontally, the sheet was focused onto multiple parts of the cone as will be shown in the results section.

Acetone Seeding

At the start of this research, it was assumed that the condensed water vapor in the compressed air would be sufficient for flow marking and visualization. After several attempts, it became obvious that there would not be enough water particles for visualization. The lack of water particles within the free-stream could be attributed to the flow moving at only Mach 2.8. It is known from past research that water vapor will condense in a Mach 3.0 flow (Arnette et al., 1995 and 1998), but will not in a Mach 2.5 flow. Based on this result, water condenses through the expansion in the nozzles at Mach numbers between 2.8 and 3.0 for the 6" by 6" wind tunnel of the AARL. Since there is an insufficient amount of condensed water particles to mark the flow, liquid acetone was used to seed the flow. The acetone is held in a pressurized tank with a spray nozzle located at the end of a high-pressure hose.

Several different nozzle locations were chosen to try to achieve optimum acetone injection. An attempt was made to inject the acetone directly into the stagnation chamber of the tunnel. This yielded only a few droplets of acetone in the free stream around the cone model. In the second effort, a six-foot length of hose was placed between the spray nozzle and the stagnation chamber. The acetone would possibly vaporize between the nozzle and the chamber. If so, it would enter the chamber as a vapor and could mix with the stagnant air more easily. This also failed to yield acceptable results. Finally, the nozzle was place directly into the high-pressure line that feeds the tunnel with air. The main airline splits at a T-connection to form two high-pressure hoses that feed the top and bottom of the tunnel. The acetone spray nozzle was placed in the center of this T-connection. Initially, this new location did not give any results. However, once the acetone tank pressure was raised to 390 psi, an acetone mist formed inside of the tunnel and images were taken. The tunnel was operated with 80 psi inside the stagnation chamber.

EXPERIMENTAL RESULTS

The original plan for this research was to acquire surface flow visualizations, Filtered Rayleigh Scattering (FRS) based flow visualizations, and quantitative flow measurements using Planar Doppler Velocimetry (PDV). These tests would be used to obtain detailed information on both the transition to turbulence and the turbulent structures in the Mach 2.8 flow over the 4:1 elliptic cone. Based on a mutual agreement between the AFOSR and the PI, a shift in the direction of the research took place midway through the project. Therefore, after preliminary results were obtained using the first two techniques, research on the elliptic cone was halted. In the Experimental Facility and Techniques section, the details of both the surface flow and FRS flow visualizations were discussed. Since no results based on PDV are to be presented, the background on PDV has been left out. Readers interested in details of PDV are referred to a recent review paper by the PI (Samimy, 1998). In the rest of this section, the surface flow visualization results will be presented followed by FRS flow visualizations.

Surface Flow Visualizations Results

As was discussed in the Experimental Facility and Techniques section, an oil-based surface flow visualization technique was employed. A 1:1:2 mixture, by volume, of Dow Corning 200 Fluid with 500 cS silicone oil, linseed oil, and Windsor & Newton Titanium White paint was used (Cattafesta et al., 1995). The purpose of using two oils of different viscosity was to simultaneously visualize regions of both high and low shear that are respectively located on the side and top surfaces (see Figure 1). The mixture of linseed oil and titanium paint marked the flow pattern on the high shear region of the side surface, while the less viscous mixture of silicone oil and titanium paint left flow marks on the low shear region of the top surface. Using either silicone oil or linseed oil with the titanium paint resulted in a limited surface flow pattern. Figure 8 shows both the top and side cone surfaces, while Figure 9 shows only the close up images of the top surface. Information on the flow regimes as well as the existence of a cross flow can be obtained from these images.

On the top surface, shown in the left image of Figure 9, one notices four distinct regions starting at the cone tip and moving downstream along the top centerline, perhaps indicating four flow regimes. The first bright region behind the tip would seem to indicate a strong cross flow region (marked 1 in Figure 9). The thin, darker, second region immediately following the first bright region seems to indicate the beginning of the transition to turbulence (marked 2). The next large, bright region seems to indicate the third region during which the flow experiences full transition to turbulence (marked 3). The more uniform, slightly darker region following the third region shows the turbulent region where the surface streamlines are parallel and there is not any

cross flow (marked 4). This is an intuitive type of interpretation that may or may not be very accurate because it is very difficult to confirm. These results indicate that the flow becomes turbulent a little over an inch from the cone tip on the centerline of the top surface. Unfortunately, the boundary layer thickness is very thin in this region and it is very difficult to use any optical diagnostics, even a FRS based technique, to visualize the flow with thin boundary layers. However, FRS results further downstream, approximately 2.1 inches from the cone tip, show the boundary layer is indeed turbulent. This corroborates the transition results from the surface visualization to some degree.

Figures 8 and 9 both show strong cross flow from the major axis toward the minor axis. As was discussed earlier, the flow direction change along the minor axis is only about 4.5°, while it is 17.5° along the major axis. This would obviously generate a strong pressure gradient, and, as a result, a strong cross flow from the major axis toward the minor axis. This cross flow is very obvious in the image of the side cone surface (left-side image - Figure 8), but not in the close up image of the top cone surface (right-side image - Figure 8). Note that the cross flow is limited to the area close to the major axis. The major portion of the top surface of the cone does not show any cross flow after the turbulent transition. Further, note that the extension and severity of cross flow will increase with Mach number, as the magnitude of the pressure gradient for the same flow turning angle will increase with Mach number. This would lead to more fluid being pushed toward the minor axis of the cone.

Filtered Rayleigh Scattering Flow Visualization Results

As was discussed earlier, the FRS technique was used to visualize the flow structure close to the cone surface. Acetone was injected into the flow far upstream of the stagnation chamber. The injected acetone evaporated and then mixed with the air before entering the nozzle. During expansion in the nozzle, the acetone condensed, and therefore, uniformly seeded the flow with particles on the order of 50 nm. The temperature increased from about 200° R in the free stream to about 500° R close to the model surface due to viscous heating. This increase caused sublimation of the acetone particles in the boundary layer and provided the contrast in the visualizations. In the images shown below, the illumination time was about 9 ns, rendering instantaneous images of the structures in the flow.

The boundary layer that developed on the cone was very thin -- on the order of a couple of millimeters at the end of the 6.0 inch cone. To enable visualization of structures in such a thin layer, the laser sheet and camera had to be focused on a small part of the cone. Figure 10 shows the location, direction, and extent of the laser sheet positions used. Figures 11 - 13 show flow streamwise flow visualizations along the cone minor axis, starting at three different downstream locations. The flow is from right to left and the Reynolds number at the beginning of Figures 11

- 13 is 3.98 x 10^6, 5.57 x 10^6, and 7.32 x 10^6, respectively. Three instantaneous images are shown in each figure. They are not correlated in time and are typical of tens of images obtained. As shown in Figure 11, the boundary layer is quite intermittent until approximately three inches from the cone tip. It seems the free stream fluid penetrates the layer almost to the surface in some areas, while there are relatively large fluid blubs in other areas. However, there is no indication of a laminar-like boundary layer or the waves associated with transitional boundary layers. It is not clear at this time whether this intermittence in the boundary layer is a characteristic of the flow, or an artifact of the visualization technique.

The boundary layer becomes less intermittent further downstream, as seen in Figure 12, and eventually becomes similar to a typical two-dimensional supersonic boundary layer, as seen in Figure 13. At the cone rear, there are some large-scale structures aligned with the downstream direction at angles on the order of 45°, similar to those in a two-dimensional supersonic boundary layer (Arnette et al., 1995 & 1998). However, there are more structures that are almost standing straight up. Whether this is typical of a three-dimensional boundary or a transitional boundary layer is not known. Figure 14 shows streamwise images 1/2 inch off-centerline starting 4.7 inches from the cone tip. The images are similar to the images in Figure 12, which were taken further upstream, along the centerline. One reason for the similarity between Figures 12 and 14 could be that the boundary layers in both cases have similar distances to develop. Another reason for the similarity could be a centerline bulging that has been noticed by other researchers in higher Mach number cases due to the cross flow effect (Kimmel et al., 1997 and Lyttle and Reed, 1995).

Figures 15 - 17 show spanwise images at three different downstream locations with Reynolds numbers of 3.34 x 10^6, 6.53 x 10^6, and 9.55 x 10^6, respectively. The flow seems to be dominated by streamwise vortices in Figure 15 with both clockwise and counter-clockwise rotation. Much further downstream, as seen in Figure 17, these structures have become 'bumps' and one cannot identify them as streamwise vortices.

The cross-flow, seen in the surface flow visualizations, could be causing the streamwise vortices noticed in Figure 15. The dark curve marked with an "A" in Figure 15 appears to be a region of space lacking acetone that has been deformed due to a cross-stream. If the cross-flow were not present the dark line would be straight. The area of the surface flow visualization of Figure 9 that corresponds to the labeled portion of Figure 15 is marked with the label "A". Thus, the majority of the FRS visualizations would not show any cross-flow since they were obtained in regions of the flow where the surface flow visualizations show straight lines.

CONCLUSIONS

The Filtered Rayleigh Scattering (FRS) optical visualization technique has been used in conjunction with an oil surface streak technique to qualitatively determine the flow pattern over a 4:1 aspect ratio elliptical cone. Both techniques were used in a conventional Mach 2.8 wind tunnel at the Ohio State University Aeronautical and Astronautical Research Laboratory. The cone configuration is the same as used by Schneider et al. (1996) in their investigation, with a cone angle on the major axis of 17.5° and 4.5° along the minor axis. The cone length is 6.3 in. The Reynolds number of 1.59×10^6 per inch is much higher than that used by Schneider et al (1996).

The purpose of studying the flow pattern over the elliptic cone was to examine the transition processes as well as the turbulent structure of a three-dimensional boundary layer after transition using advanced optical diagnostics. With mutual agreement of the AFOSR and the Principal Investigator, the research direction was changed midway through the research. Therefore, the findings of this report are preliminary with no further research planned.

Both surface flow visualizations and Filtered Rayleigh Scattering (FRS) based flow visualizations were used in this study. The results showed that the boundary layer developing along the major centerline of the cone, the flattest region of the cone, underwent transition to turbulence within one and a half inches of the cone tip. Surface cross flow was observed primarily near the minor centerline of the cone, which is the area with the largest curvature. No cross flow was observed around the major centerline after approximately one-half inch downstream of the cone tip. The FRS flow visualizations showed that the post-transition flow was dominated by large structures in the developing region of the turbulent boundary layer. The developing boundary layer was random in nature; meaning that either there was or was not a measurable boundary layer on the surface. Farther downstream, the boundary layer appeared to be similar to a two-dimensional supersonic boundary layer. The boundary layer was slightly thicker at the centerline. However, a bulging of the boundary layer at the centerline, which had been observed by previous researchers in higher Mach number experiments, was not noticed in the present experiments.

ACKNOWLEDGMENTS

This work was sponsored in part by the Air Force Office of Scientific Research (AFOSR) under grant/contract number F49620-97-1-0088. The views and conclusions contained herein are those of the authors and should not be interpreted as necessarily representing the official policies or endorsements, either expressed or implied, of the Air Force Office of Scientific Research or the U.S. Government.

REFERENCES

Arnette, S.A., Samimy, M., and Elliott, G.S., "The Effects of Expansion Regions on the Turbulence Structure of a Supersonic Boundary Layer," Journal of Fluid Mechanics, 1998, 367: 67-105.

Arnette, S.A., Samimy, M., and Elliott, G.S., "Structure of a Supersonic Boundary Layer after Various Regions of Expansions," AIAA Journal, 1995, 33: 430-438.

Cattafesta III, L.N., Iyer, V., Masad, J.A., King, R.A., and Dagenhart, J.R., "Three-Dimensional Boundary Layer Transition on a Swept Wing at Mach 3.5," 1995, 33: 2032-2037.

Huang, S.L, Stuckert, G.K., and Herbert, Th., "Cross Flow Instability of the Supersonic Flow over a 4:1 Elliptic Cone," Final Report, Contract F49620-94-C-0053, AFOSR, January 1995.

Kim, J.-H., 1998, "An Experimental Study of Mixing and Noise in a Supersonic Rectangular Jet with Modified Trailing Edges," Ph.D. Dissertation, Department of Mechanical Engineering, The Ohio State University.

Kimmel, R.L., Klein, M.A., and Schwoerke, S.N., "Three-Dimensional Hypersonic Laminar Boundary Layer Computations for Transition Experiment Design," Journal of Aircraft and Rockets, 1997, 34:409-415.

King, R.A., "Three-Dimensional Boundary Layer Transition on a Cone at Mach 3.5," Experiments in Fluids, 1992, 13: 305-314.

Lyttle, I.J and Reed, H.L., "Use of Transition Correlations for Three-Dimensional Boundary Layers Within Hypersonic Flows," AIAA Paper 95-2293, 1995.

Miles, R.B. and Lempert, W.R., "Flow Diagnostics in Unseeded Air," AIAA Paper 90-0624, 1990.

Pope, A., Goin, K.L., 1965, High Speed Wind Tunnel Testing, Wiley.

Reed, H.L. and Haynes, T.S., "Transition Correlations in Three-Dimensional Boundary Layers," AIAA Journal, 1994, 32: 923-929.

Samimy, M., "A Review of Planar Multiple-Component Velocimetry in High Speed Flows (Invited Paper)," AIAA Paper 98-2509, 1998.

Samimy, M. Elliott, G.S., "Effects of Compressibility on the Characteristics of Free Shear Layers," AIAA Journal, 1990, 28: 439-445.

Smits, A.J., "Rayleigh Imaging of Mach 8 Boundary Layer Flow Around an Elliptic Cone Body," AFOSR Turbulence and Internal Flows/Unsteady Aerodynamics and Hypersonic Contractor Meeting, August 1998.

Schneider, S.P., Collicott, S.H., Schmisseur, J.D., Ladoon, D., Randall, L., Munro, S.E., and Sayler, T.R., "Laminar Turbulent Transition Research in the Purdue Mach-4 Quiet-Flow

Ludwieg Tube," AIAA Paper 96-2191, 1996.

Settles, G.S. and Teng, H.-Y., 1983, "Flow Visualization Methods for Separated three-dimensional Shock Wave/Turbulent Boundary-Layer Interactions," AIAA Journal, Vol. 21, No. 3, 390-397.

TRC Thermodynamic Tables (Non-Hydrocarbons), 1975, ka-190.

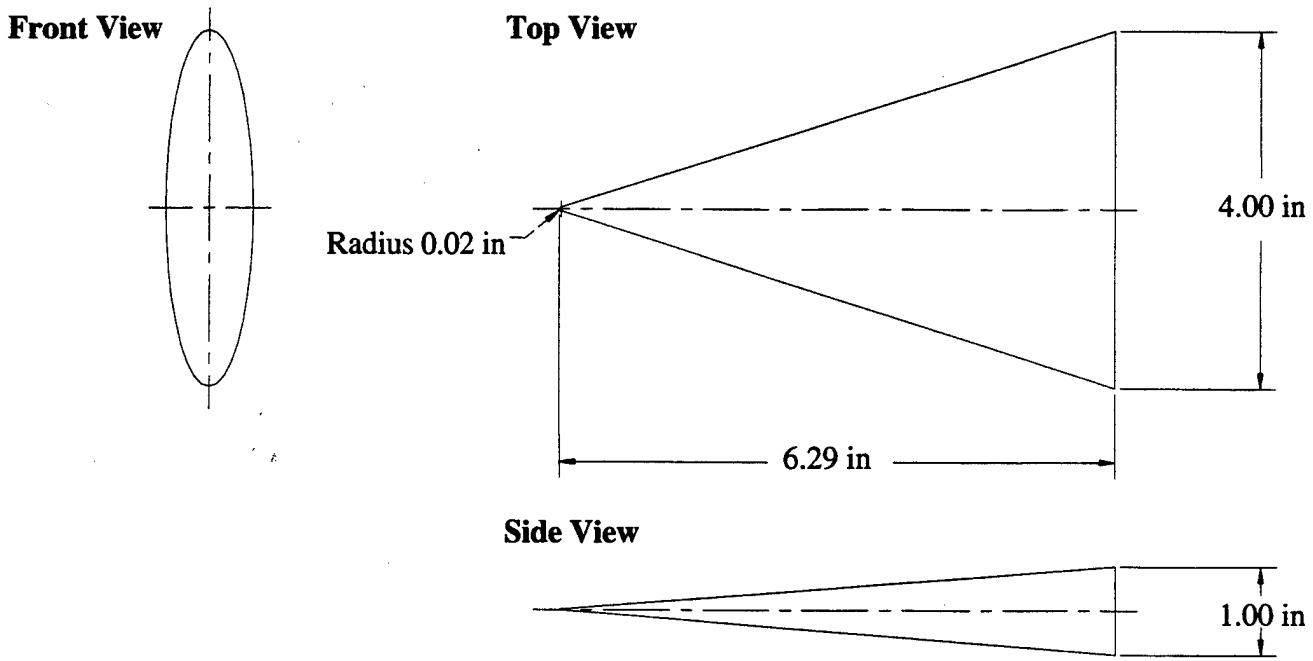

Figure 1 Dimensions of the Elliptical Cone Model

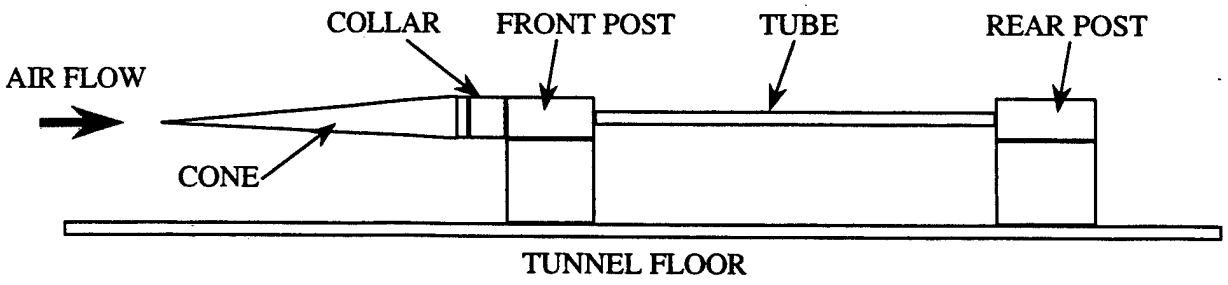

Figure 2 Schematic of Cone Model with Two-Piece Support

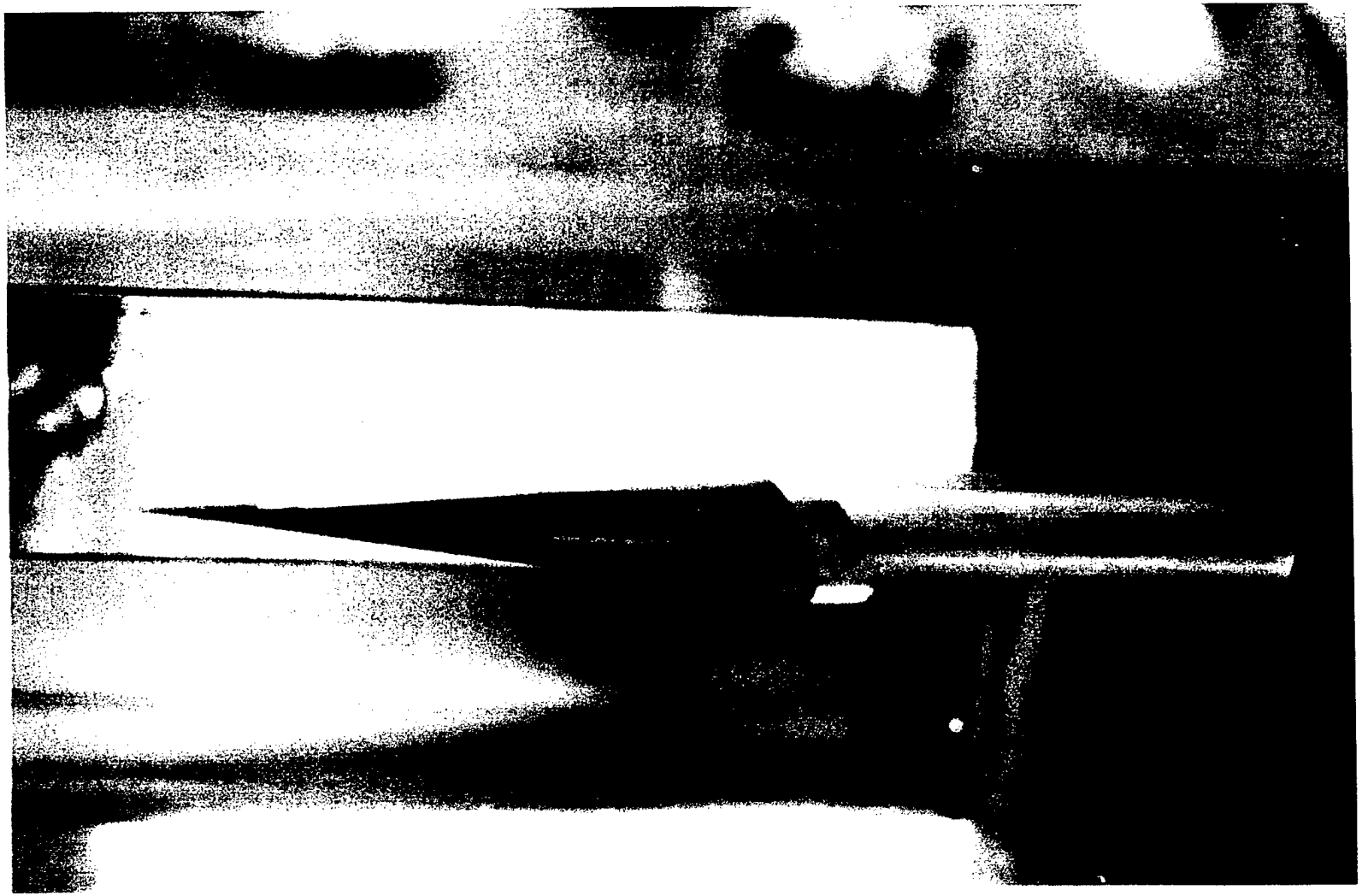

Figure 3 Elliptical Cone Model in the Wind Tunnel with the One-Piece Support

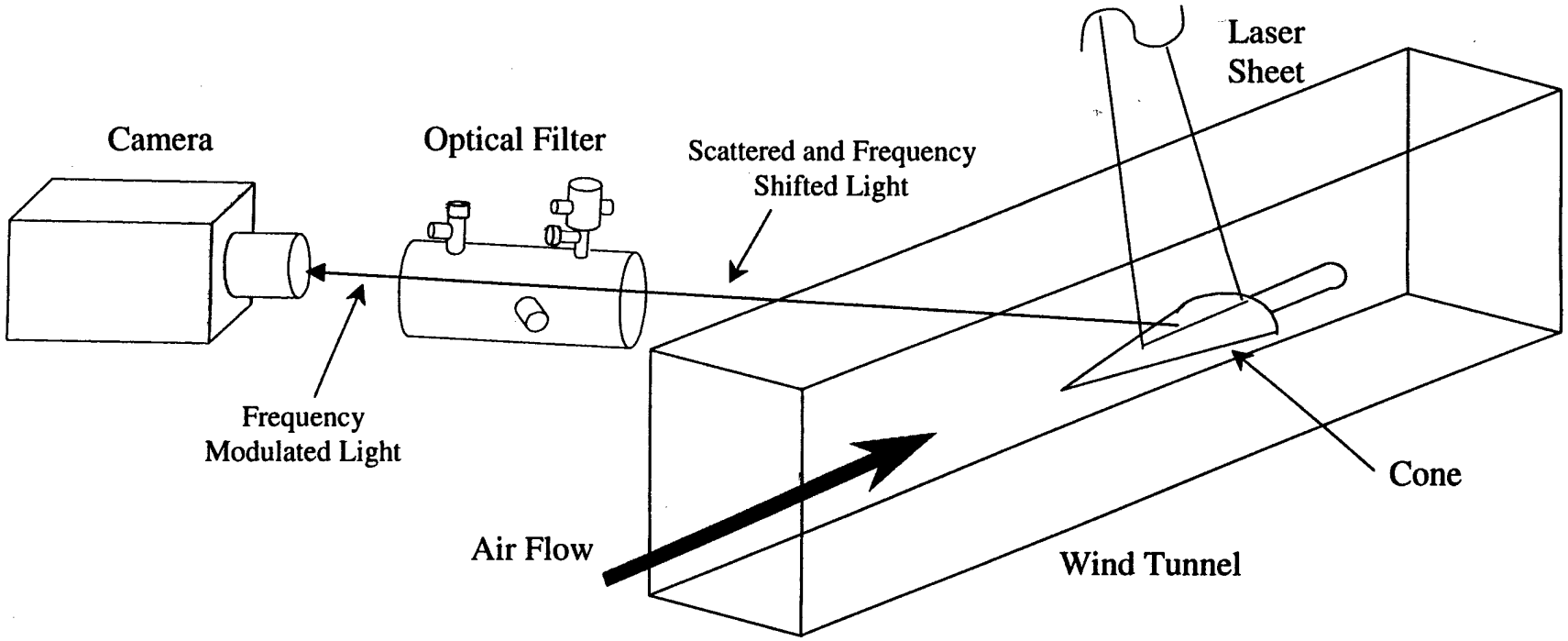

Figure 4 Experimental Arrangement showing Cone Model in Wind Tunnel with the Optical Filter and ICCD Camera

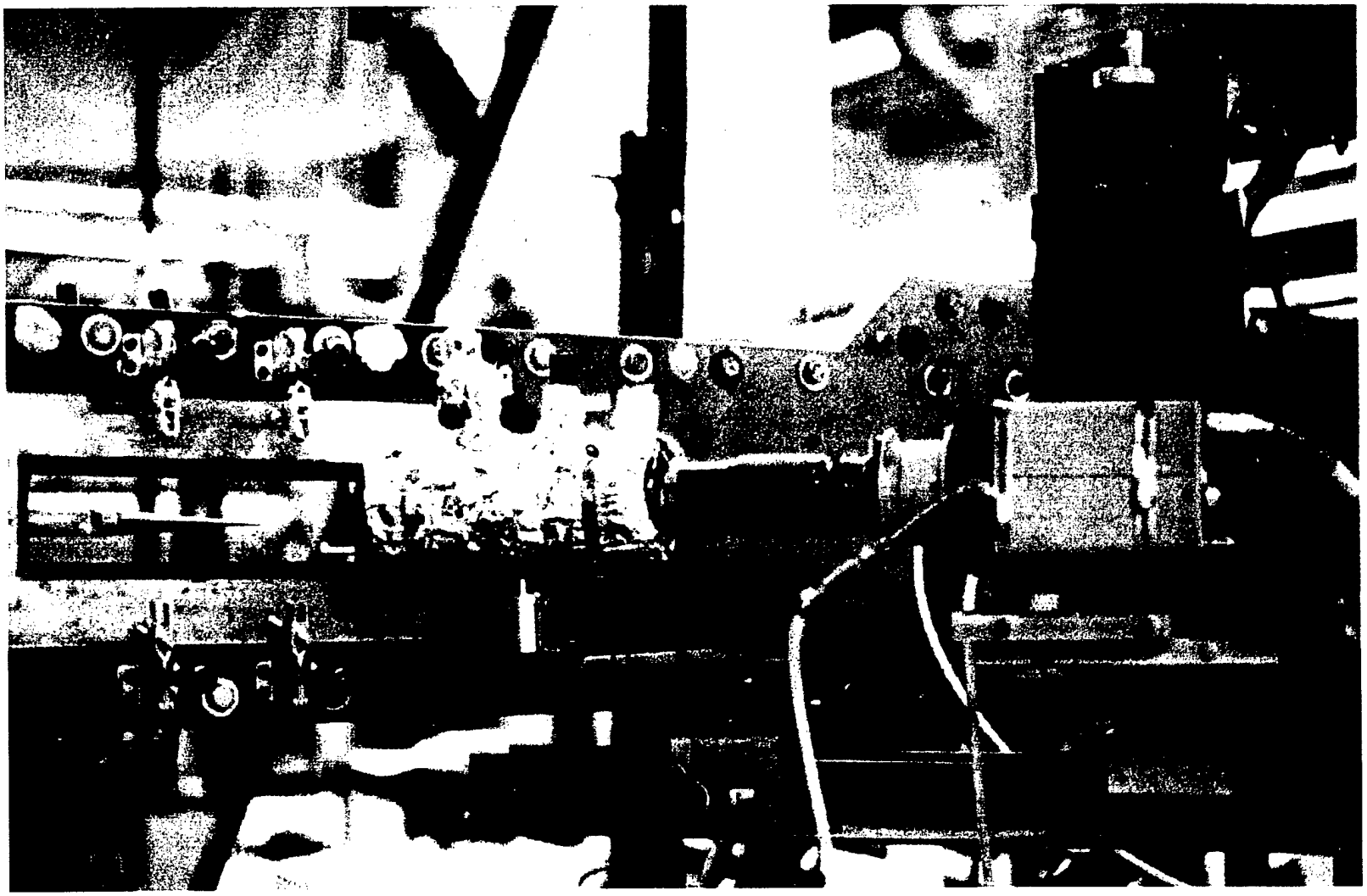

Figure 5 Opitcal Filter and ICCD Camera with Orientation relative to the Wind Tunnel and Cone Model

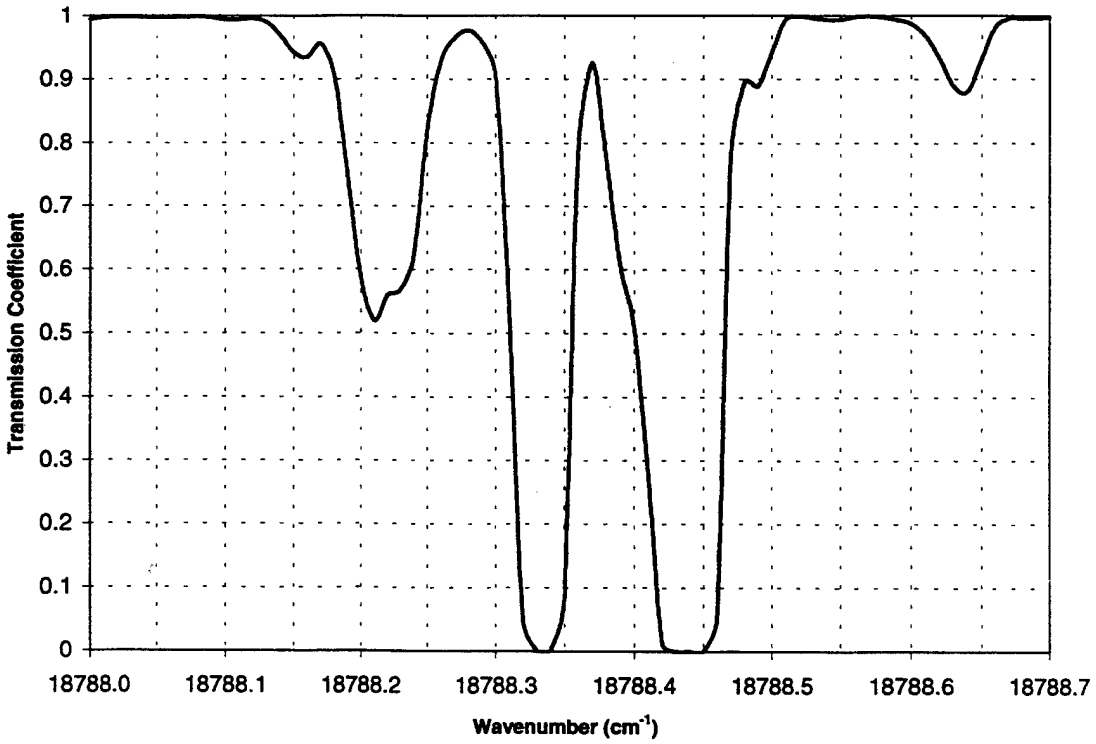

Figure 6 Theoretical Optical Filter Profile for the Molecular Iodine Filter

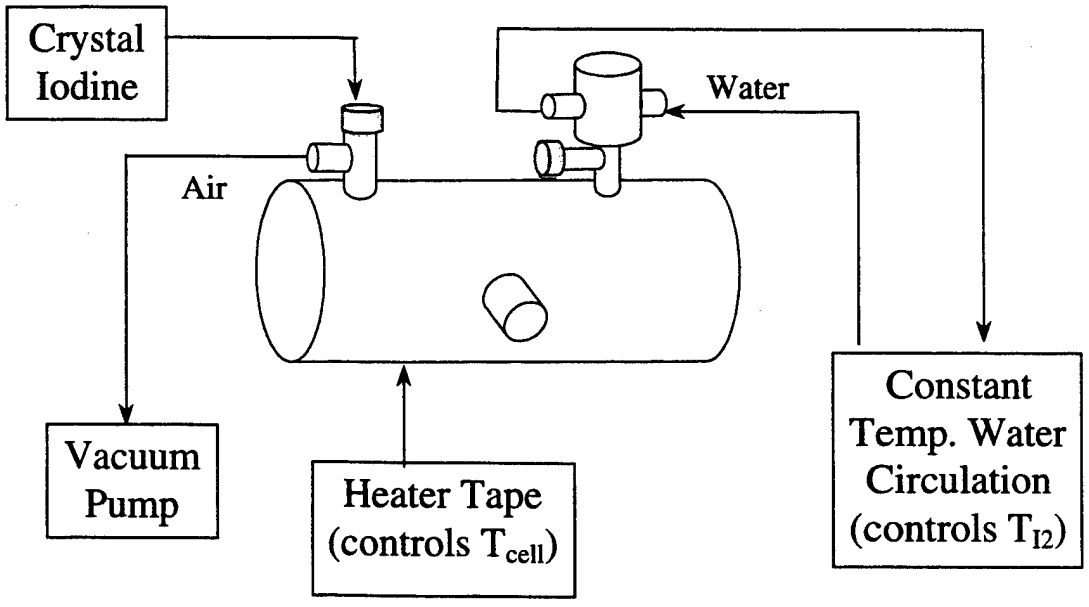

Figure 7 Optical Filter and the Operations Performed during Preparation

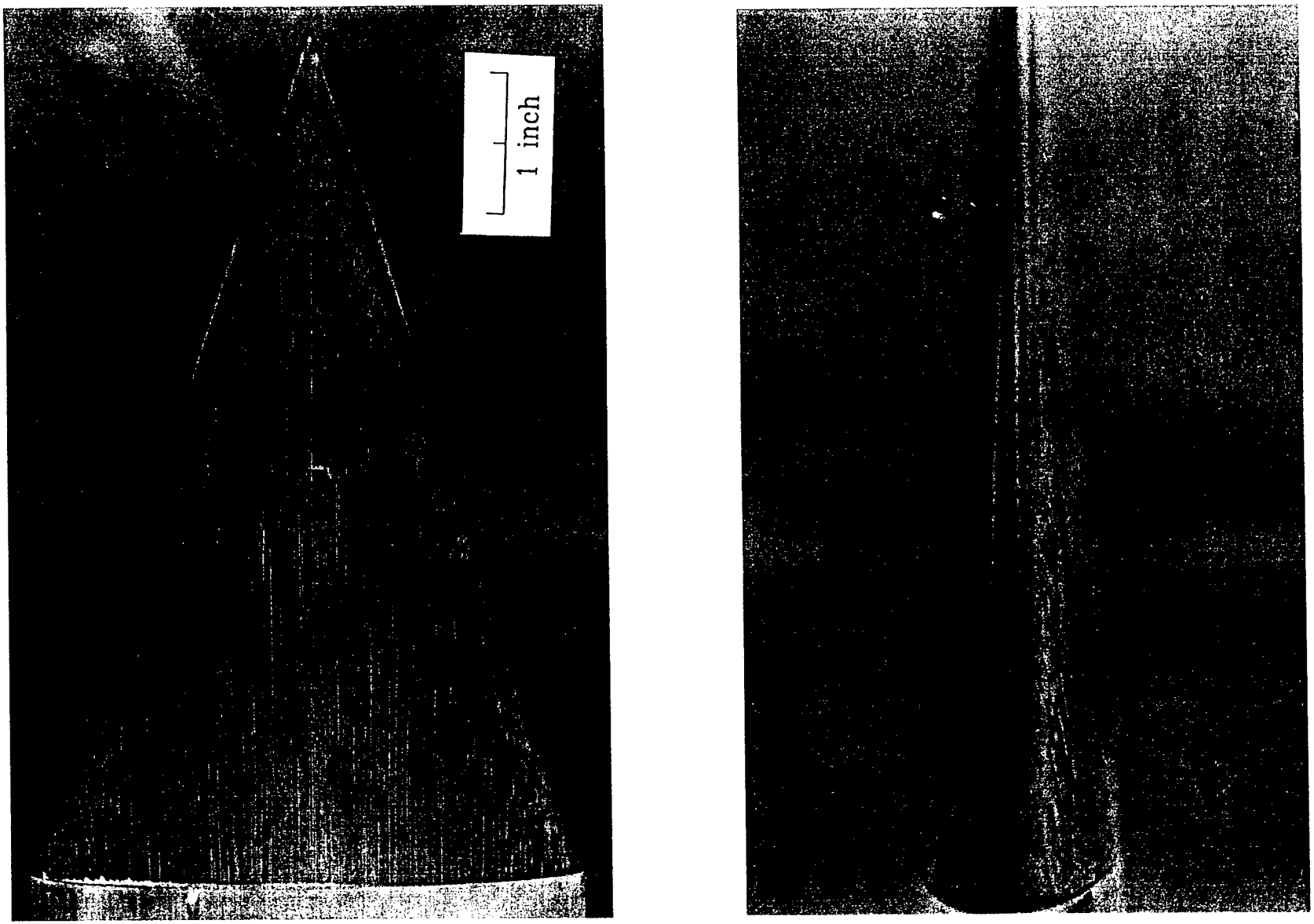

Figure 8 Surface Flow Visualization using Streak Technique

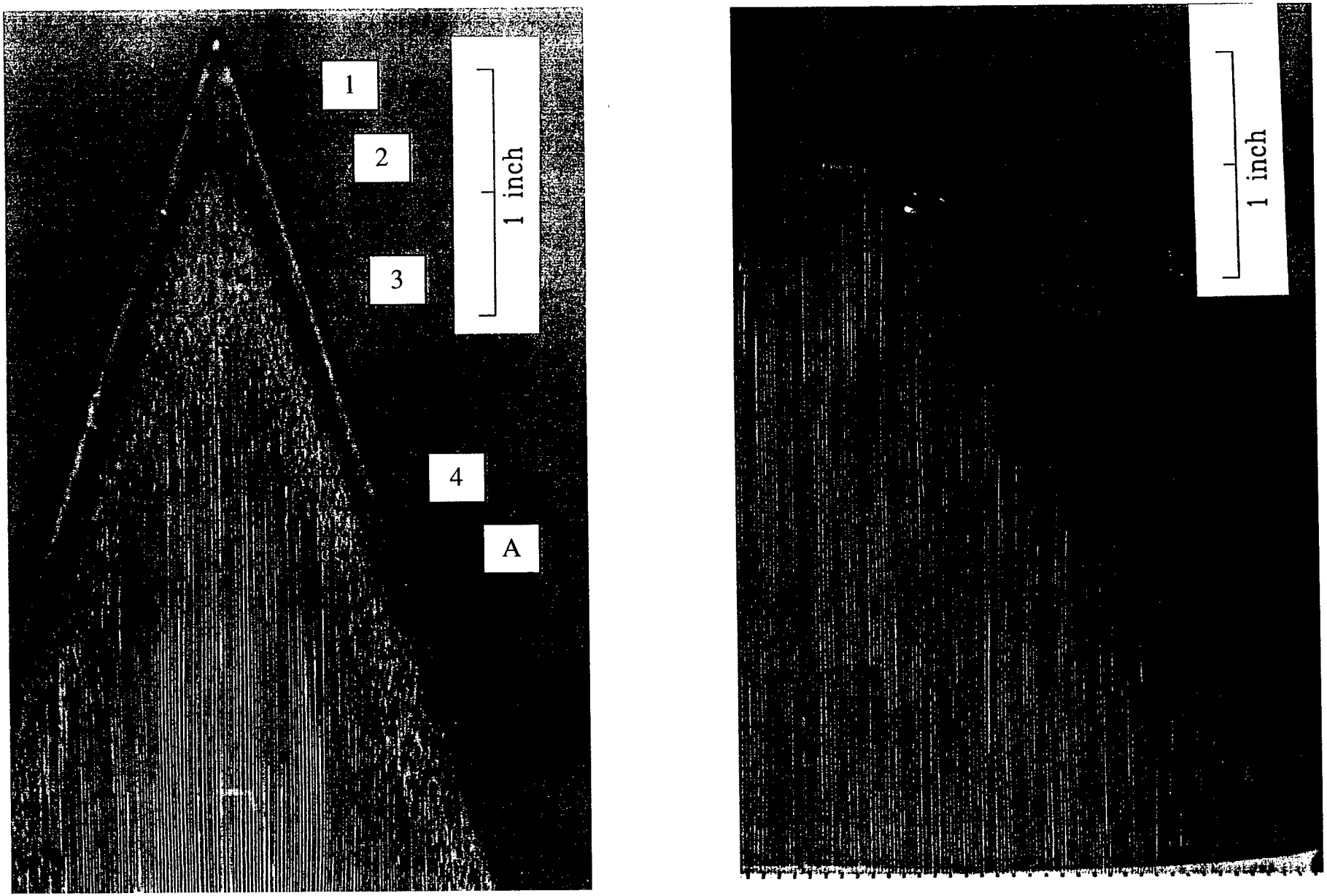

Figure 9 Surface Flow Visualization using Streak Technique

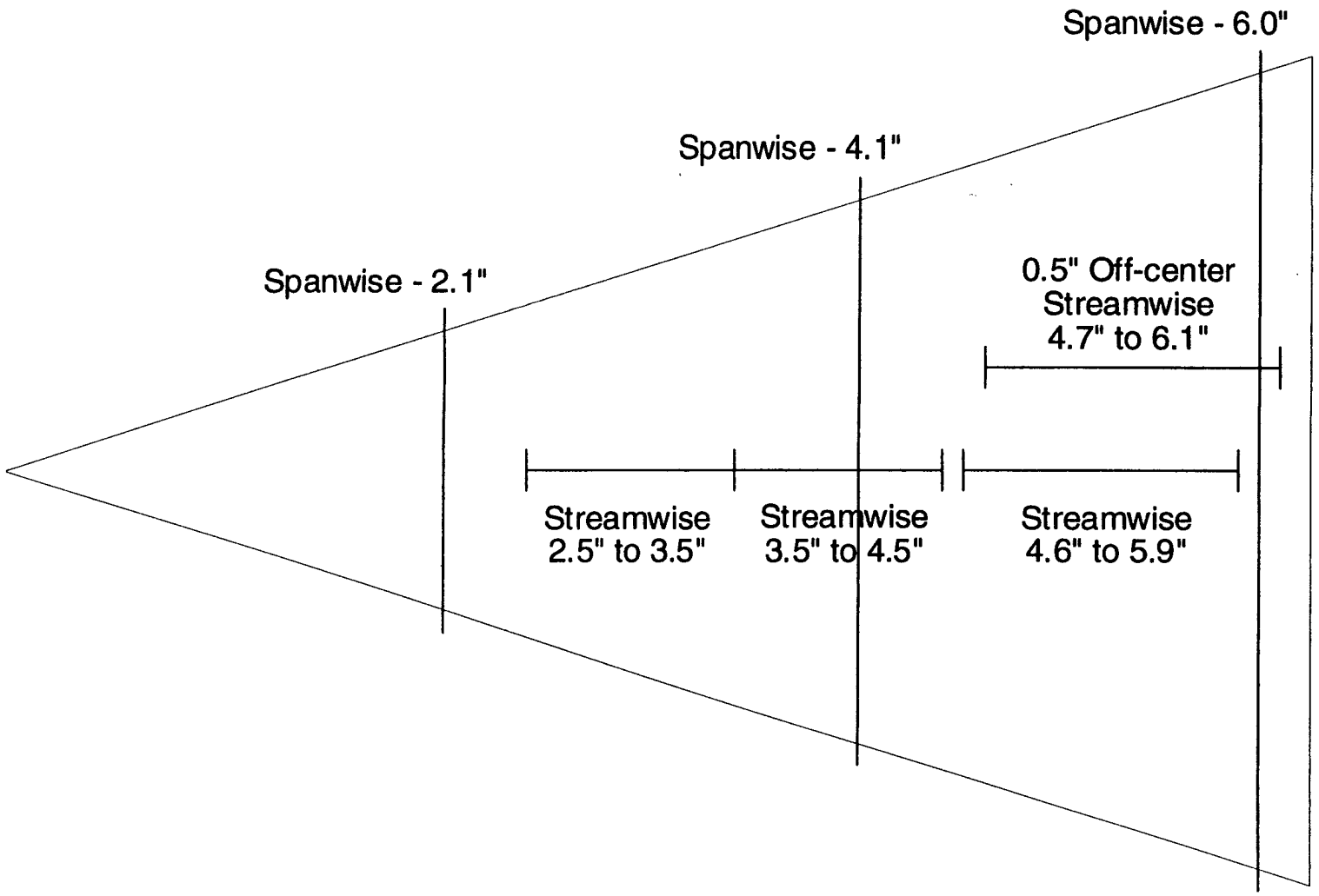

Figure 10 Top View of Cone showing Laser Sheet Positions used to Obtain FRS Visualizations

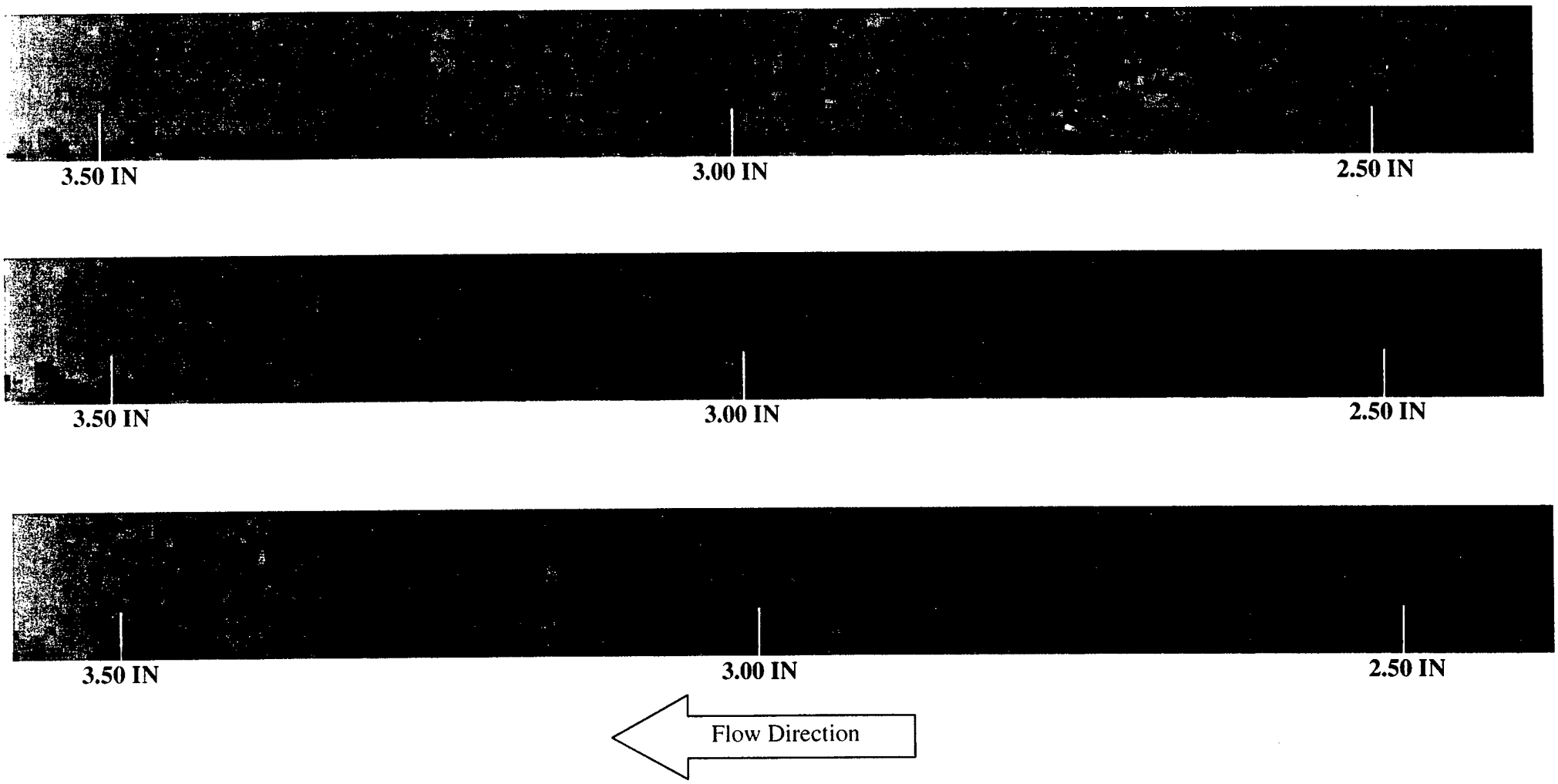

Figure 11 FRS Flow Visualization for Centerline Streamwise Position, Distances are from Cone Tip

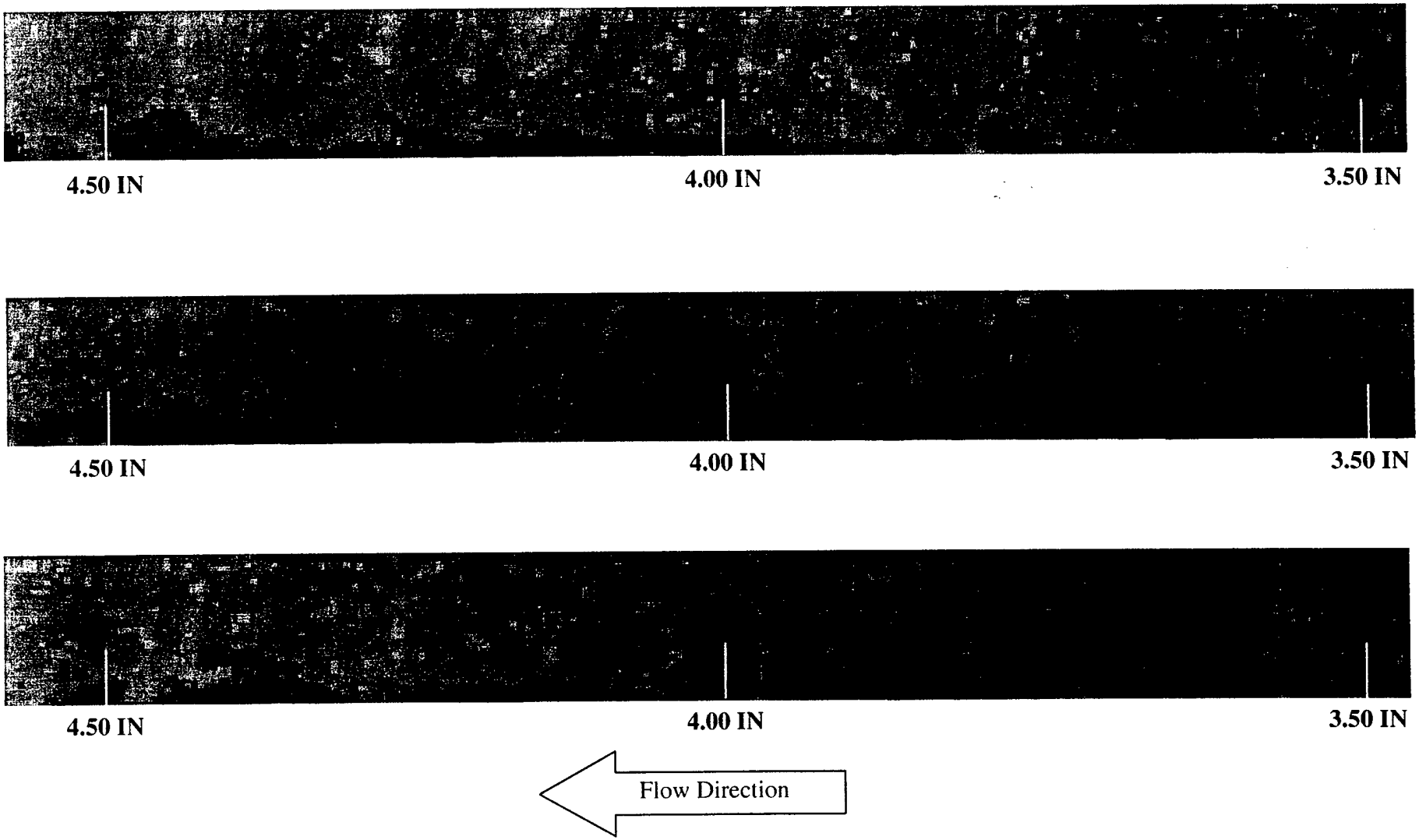

Figure 12 FRS Flow Visualization for Centerline Streamwise Position, Distances are from Cone Tip

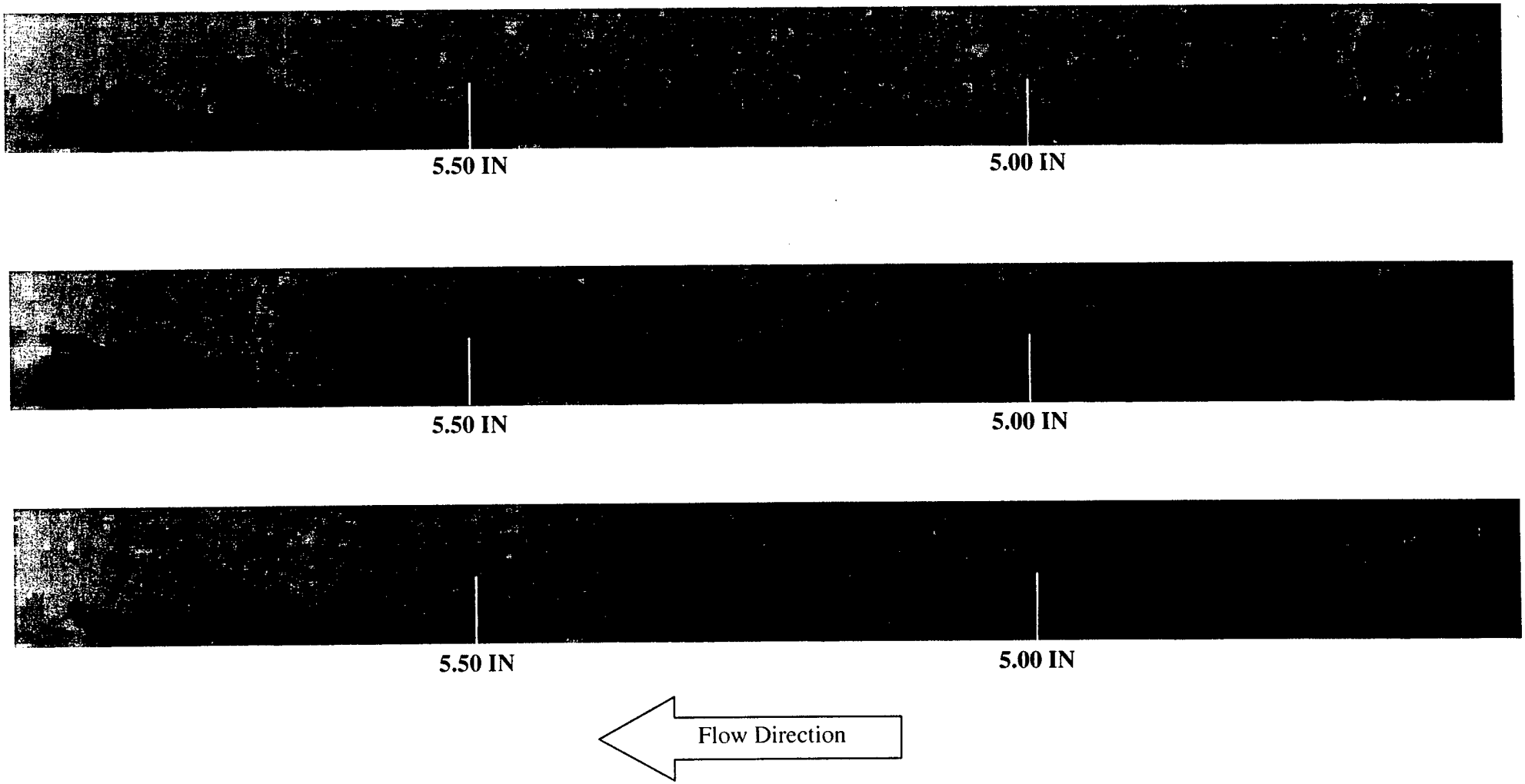

Figure 13 FRS Flow Visualization for Centerline Streamwise Position, Distances are from Cone Tip

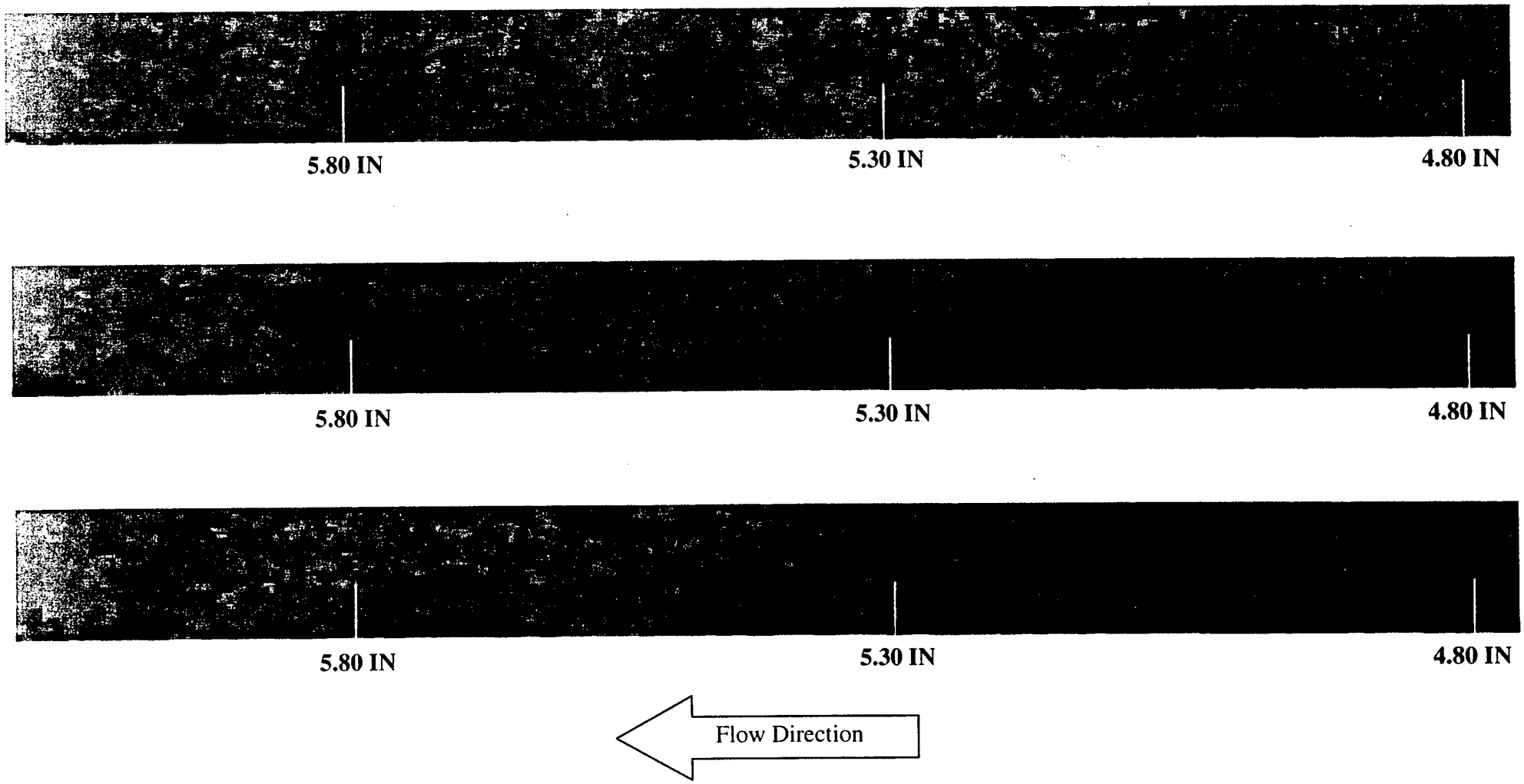

Figure 14 FRS Flow Visualization for ½ Inch Off-Centerline Streamwise Position, Distances are from Cone Tip as Measured at the Centerline

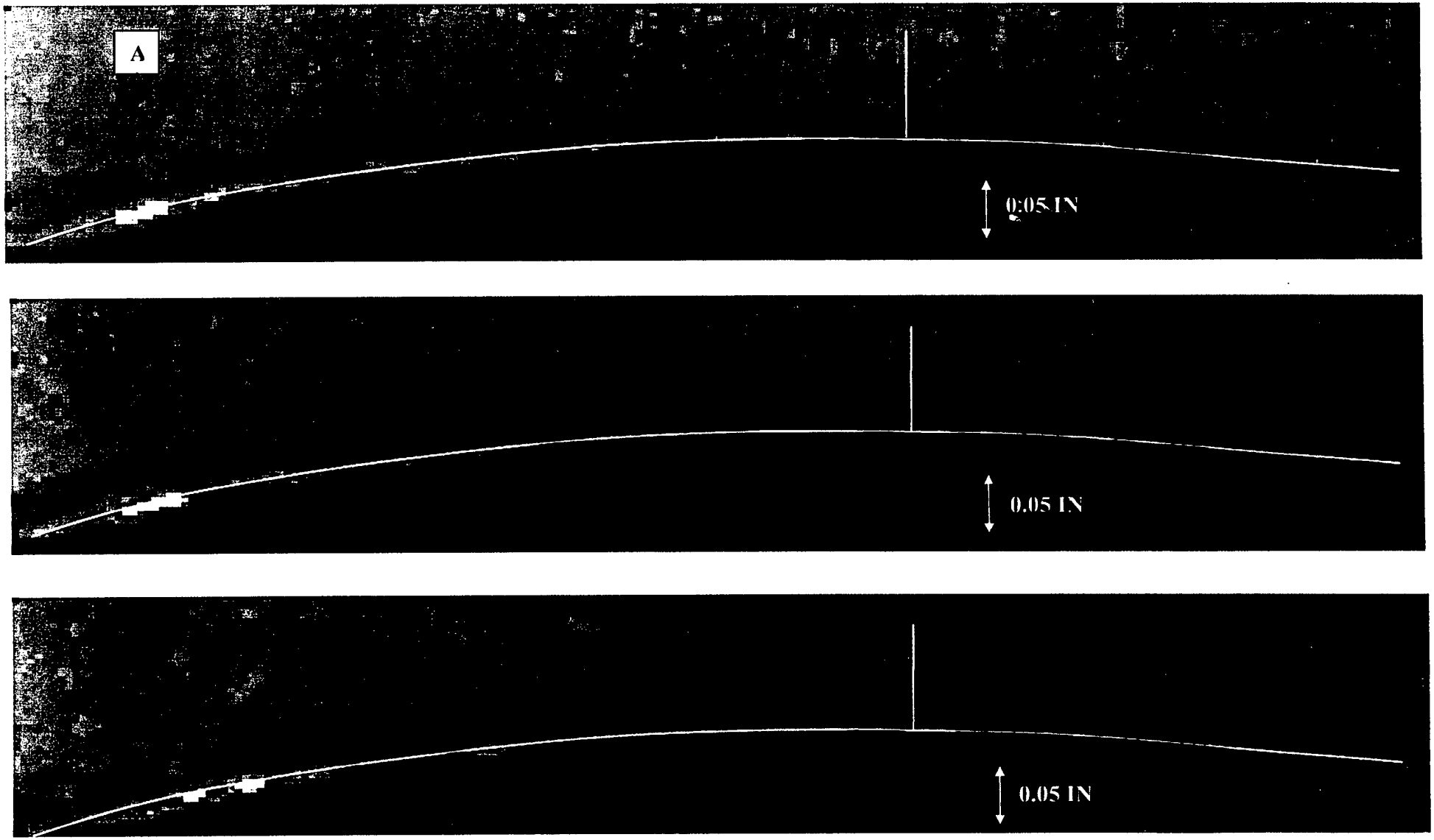

Figure 15 FRS Flow Visualization for Spanvise Position 2.1 Inches from the Cone Tip

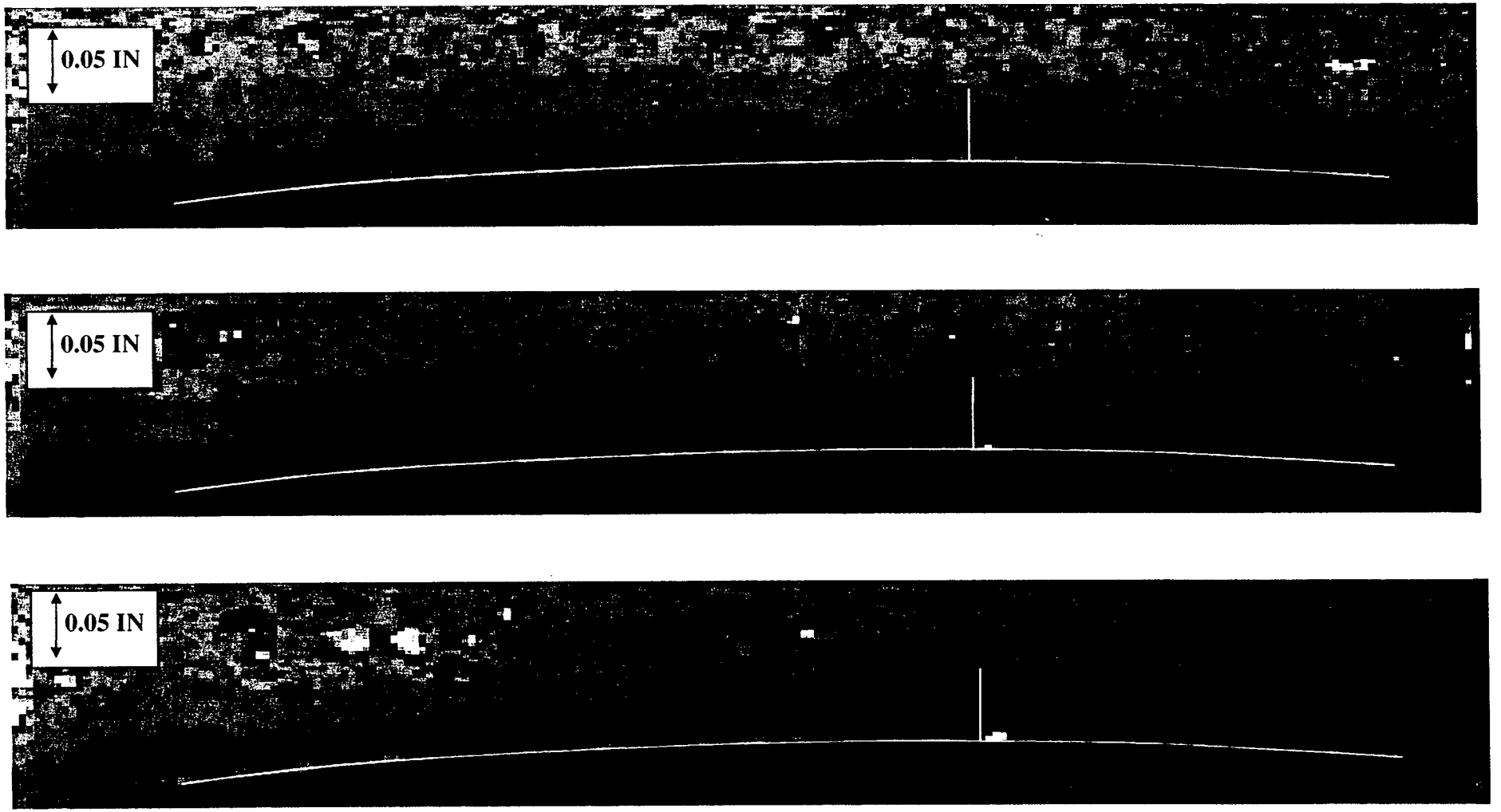

Figure 16 FRS Flow Visualization for Spanwise Position 4.1 Inches from the Cone Tip

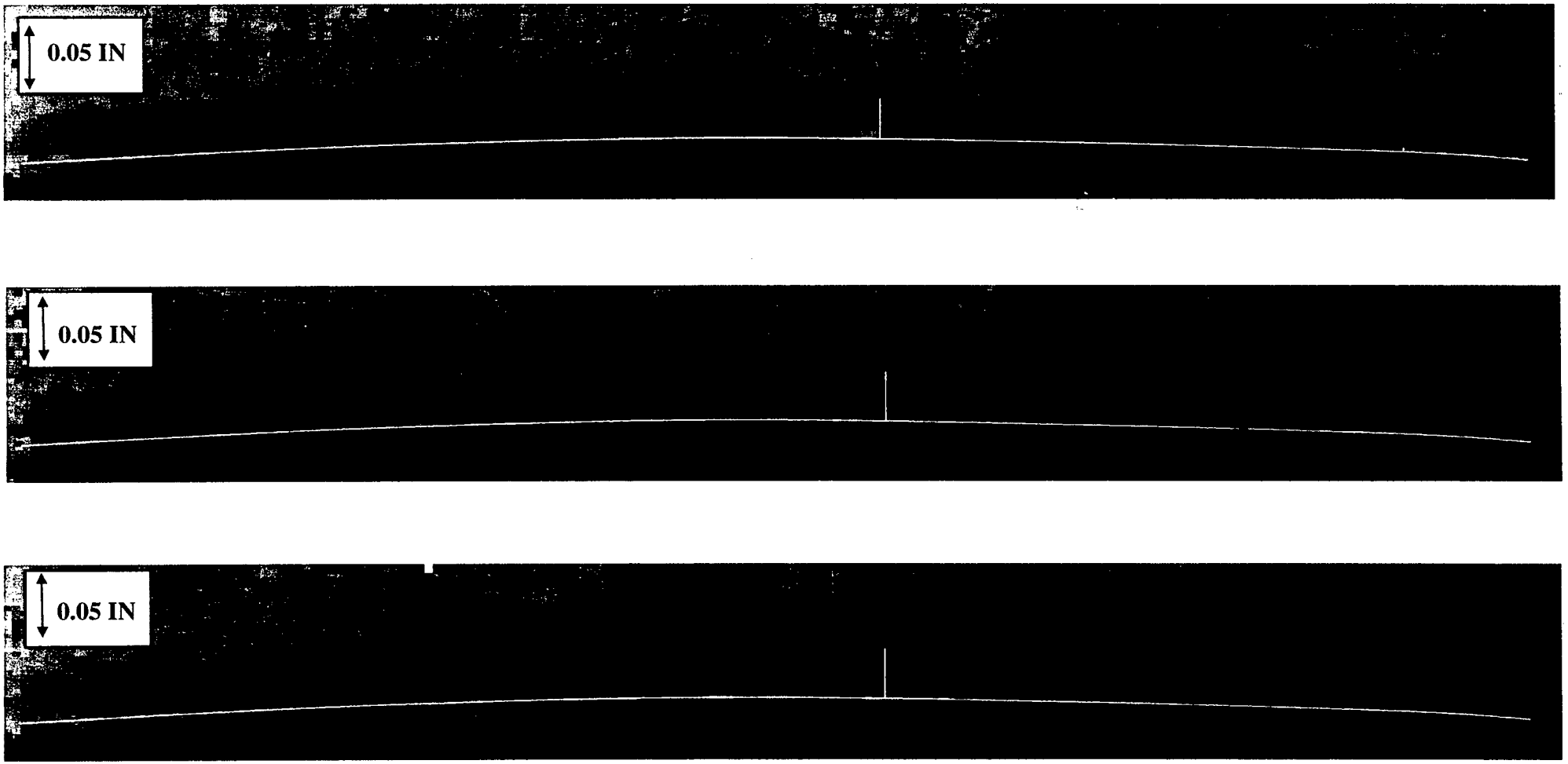

Figure 17 FRS Flow Visualization for Spanwise Position 6.0 Inches from the Cone Tip